

## Photocatalytic reduction of NO with NH<sub>3</sub> using Si-doped TiO<sub>2</sub> prepared by hydrothermal method

Ruiben Jin, Zhongbiao Wu\*, Yue Liu, Boqiong Jiang, Haiqiang Wang

Department of Environmental Engineering, Zhejiang University, Hangzhou 310027, China

### ARTICLE INFO

#### Article history:

Received 26 November 2007  
Received in revised form 12 March 2008  
Accepted 12 March 2008  
Available online 20 March 2008

#### Keywords:

Photocatalytic reduction  
Nitric oxide  
Hydrothermal method  
Si/TiO<sub>2</sub>

### ABSTRACT

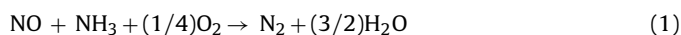
A series of Si-doped TiO<sub>2</sub> (Si/TiO<sub>2</sub>) photocatalysts supported on woven glass fabric were prepared by hydrothermal method for photocatalytic reduction of NO with NH<sub>3</sub>. The photocatalytic activity tests were carried out in a continuous Pyrex reactor with the flow rate of 2000 mL/min under UV irradiation (luminous flux:  $1.1 \times 10^4$  lm, irradiated catalyst area: 160 cm<sup>2</sup>). The photocatalysts were characterized by X-ray diffraction (XRD), BET, X-ray photoelectron spectroscopy (XPS), Fourier transform infrared (FT-IR) spectrophotometer, transmission electron microscopy (TEM), photoluminescence (PL) and temperature-programmed desorption (TPD). The experiment results showed that NO conversion on Si/TiO<sub>2</sub> at 323 K could exceed 60%, which was about 50% higher than that on Degussa P25 and pure TiO<sub>2</sub>. With the doping of Si, photocatalysts with smaller crystal size, larger surface area and larger pore volume were obtained. It was also found that Ti–O–Si bands were formed on the surface of Si/TiO<sub>2</sub> and that the surface hydroxyl concentration was greatly increased. As a result, total acidity and NH<sub>3</sub> chemisorption amount were enhanced for Si/TiO<sub>2</sub> leading to its photocatalytic activity improvement.

© 2008 Elsevier B.V. All rights reserved.

### 1. Introduction

NO<sub>x</sub>, mainly nitric oxide, is a typical air pollutant, which can cause town smog and acid rain. Various processes, including combustion modifications, dry processes, and wet processes, are under operation to remove NO<sub>x</sub> from stationary sources. Selective catalytic reduction (SCR) has been reported to be a prospective de-NO<sub>x</sub> process over TiO<sub>2</sub>-based catalysts because of its high efficiency [1,2].

Currently, photocatalytic process for the reduction of NO has been studied since it decreases reaction temperature, operating cost and energy consumption [3]. Teramura et al. [4] developed a photoassisted de-NO<sub>x</sub> (photo-SCR) process with NH<sub>3</sub> which could proceed at room temperature over TiO<sub>2</sub> surface under photoirradiation. The reasonable reaction mechanism of the photo-SCR was demonstrated and the total reaction was described as follows:



The photoactivity was found to be directly related to the catalyst acidity by Yamazoe et al. [5]. Larger the catalyst acidity is, larger the NH<sub>3</sub> chemisorption amount is. The larger NH<sub>3</sub> adsorption amount leads to the higher surface concentration of amide radical as well as nitrosoamide species. However, few studies to increase the acidity

of photo-SCR catalyst have been performed. Therefore, it is of significance to make more modifications to develop more acid sites for the photocatalysts and enhance their photocatalytic activity in photo-SCR reaction.

It has been observed that doping Si in TiO<sub>2</sub> photocatalyst was an effective way to improve the catalyst photoactivity and acidity. Tanabe et al. [6] dealt with silica/titania mixed oxides and concluded that Brønsted acidity would be developed in the SiO<sub>2</sub>-rich region while Lewis acidity would be developed in the TiO<sub>2</sub>-rich region. Bonelli et al. [7] has also found that the interaction between titania and silica in TiO<sub>2</sub>/SiO<sub>2</sub> occurred on supported Ti<sup>4+</sup> sites and the prepared catalysts had sufficient Lewis acid sites.

Thus, silica-modified TiO<sub>2</sub> would be a potential high activity photocatalyst for the reduction of NO. Several methods have been reported on the preparation of SiO<sub>2</sub>-TiO<sub>2</sub> mixed oxides [8–10]: mixing particles of both preformed oxides, attaching TiO<sub>2</sub> onto mesoporous silica, and either hydrothermal co-precipitation or co-gelation from the corresponding titania and silica precursors. The main purpose of this paper was to develop a high photo-SCR activity silica-doped TiO<sub>2</sub>. Hydrothermal method was used for photocatalyst preparation in this work, since it has been reported to be an effective technique to prepare TiO<sub>2</sub> particles of desired size and shape with homogeneity in composition as well as a high degree of crystallinity [11]. And X-ray diffraction (XRD), X-ray photoelectron spectroscopy (XPS), Fourier transform infrared (FT-IR) spectrophotometer, NH<sub>3</sub> temperature-programmed desorption (NH<sub>3</sub>-TPD), transmission electron microscopy (TEM), photoluminescence

\* Corresponding author. Tel.: +86 571 87952459; fax: +86 571 87953088.  
E-mail address: [zbwu@zju.edu.cn](mailto:zbwu@zju.edu.cn) (Z. Wu).

(PL) and UV–vis diffuse reflectance spectra (UV–vis DRS) measurements were used to clarify the relationship between the changes in physicochemical properties and the enhancement of photoactivity when Si was doped.

## 2. Experimental

### 2.1. Catalyst preparation

The hydrothermal process was developed in the lab and precursor sols for silica-doped TiO<sub>2</sub> were prepared using tetrabutyl titanate Ti(OC<sub>4</sub>H<sub>9</sub>)<sub>4</sub> and ethyl silicate (C<sub>2</sub>H<sub>5</sub>)<sub>4</sub>SiO<sub>4</sub> as raw materials. Ethanol C<sub>2</sub>H<sub>5</sub>OH was used as solvent. The molar ratio of Ti(OC<sub>4</sub>H<sub>9</sub>)<sub>4</sub>:(C<sub>2</sub>H<sub>5</sub>)<sub>4</sub>SiO<sub>4</sub>:C<sub>2</sub>H<sub>5</sub>OH:H<sub>2</sub>O in the mixed solution was 1:*x*:20:40, where *x* stands for the Si/Ti molar ratio.

The sols were obtained after stirring the solution for 1 h at room temperature and then were transferred to a 100 mL stainless-steel autoclave covered with Teflon for hydrothermal treatment (temperature: 473 K, time: 12 h). After the hydrothermal treatment, the autoclave was cooled down to room temperature quickly. The precipitate was washed by ethanol and water for three times and then separated by centrifugation (4000 rpm, 20 min). The collected particles were dispersed in ethanol to make 5 wt% suspensions for the next dip-coating process. The immobilization of catalyst was carried out by dip-coating method and the woven glass fabric was used as catalyst support. The woven glass fabric was supplied by Hangzhou woven glass fabric factory (thickness: 0.5 mm; filament diameter: 9 μm). In all experiments, the weight of coated TiO<sub>2</sub> was 0.5 g ± 10%. The samples thus prepared were labeled as Si(*x*)/TiO<sub>2</sub>. Pure TiO<sub>2</sub> catalyst was prepared by the same method without the addition of ethyl silicate and Degussa P25 was chosen as standard for comparison.

### 2.2. Characterization

XRD patterns were obtained by using Cu Kα radiation, using a Rigaku D/MAX RA instrument at 40 kV and 150 mA with the angle of 2θ from 20° to 80°. The surface areas were measured by N<sub>2</sub> adsorption by the BET method using a Micromeritics ASAP 2020 instrument. XPS was used to analyze the atomic surface state on each catalyst with a V.G. Scientific Escalab 250 with Al Kα X-rays. The concentration of Ti, Si and O on the surface of the samples was

calculated from the ratio of peak areas of the XPS data of the samples. Fourier transform infrared spectrometry (Nicolet Nexus 670) with an effective wavenumber range of 400–4000 cm<sup>-1</sup> was used to analyze the groups on the surface of catalysts. The morphology of TiO<sub>2</sub> particles was examined by transmission electron microscopy and high-resolution TEM (HR-TEM) using a JEM-2010 instrument. For photoluminescence measurements, a xenon UV–vis–near-IR excitation lamp with the excitation wavelength of 300 nm was used. The PL signal was detected by a Steady-state/Lifetime Spectrofluorometer (Fluorolog-3-Tau, Jobin Yvon) at room temperature. The UV–vis diffuse reflectance spectra were taken using a UV–vis spectrophotometer (TV-1901) to determine the catalysts wavelength distribution of the absorbed light.

NH<sub>3</sub>-TPD was used to determine the total acidity of the photocatalysts. The experiments were performed on a custom-made TCD setup. Before the experiment, 100 mg sample was pretreated in He at 773 K for 1 h to remove adsorbed H<sub>2</sub>O and other gases. After the furnace was cooled down to room temperature, the sample was treated with anhydrous NH<sub>3</sub> (4% in He) at a flow rate of 30 mL/min for about 30 min. Subsequently, the catalyst was purged into a He flow at 323 K until a constant baseline level was attained. Desorption was carried out by heating the sample in He (30 mL/min) from 323 to 973 K at a heating rate of 5 K/min.

### 2.3. Photocatalytic activity measurement

Photocatalytic reduction of NO with NH<sub>3</sub> was carried out in a continuous flow reactor. The schematic experimental setup is shown in Fig. 1. Photocatalyst coated on the woven glass fabric was set into a Pyrex reactor with a volume of 200 mL. Photocatalyst was irradiated by two 250 W high-pressure Hg lamps (Philips). The wavelength of the Hg-arc lamp varied in the range from 300 to 400 nm with the maximum light intensity at 365 nm, the luminous flux was 1.1 × 10<sup>4</sup> lm and the irradiated catalyst area was 160 cm<sup>2</sup>. The reactant gas feed typically consisted of 400 ppm NO, 400 ppm NH<sub>3</sub>, 3% O<sub>2</sub> and the balance N<sub>2</sub>. The flow rate was 2000 mL/min and the temperature of the reactor was held at 323 K. The UV light was turned on when the adsorption equilibrium was reached which meant the NO concentration outlet was equal to that of inlet. Both the inlet and outlet NO concentrations were analyzed by a flue gas analyzer (Testo 335). Not only NO conversions but also photocatalytic rates of different catalysts were calculated to

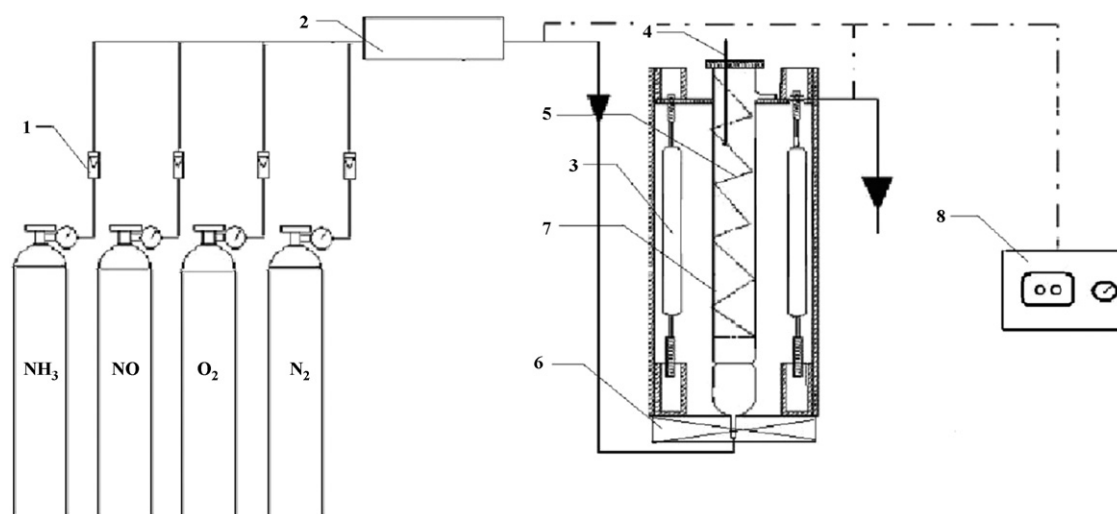


**Fig. 1.** Schematic diagram of the photocatalytic reduction equipment. (1) Flow meter; (2) gas mixer; (3) Hg-arc lamp; (4) thermocouple; (5) catalyst; (6) fan; (7) Pyrex reactor; (8) gas analyzer.

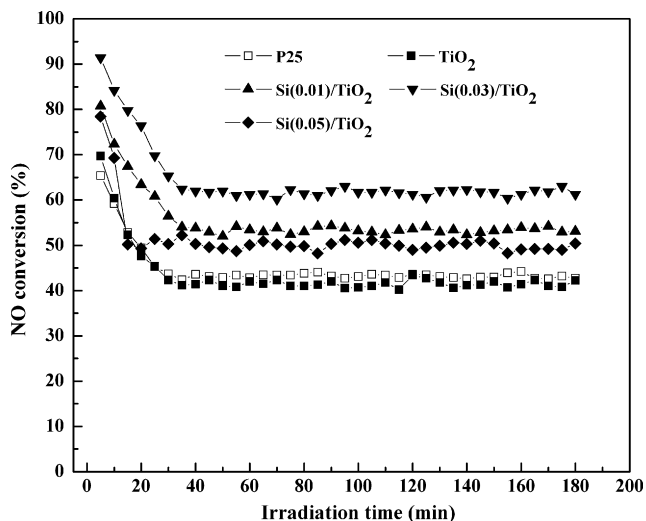


**Fig. 2.** Photocatalytic reduction efficiency of NO on P25, TiO<sub>2</sub> and Si/TiO<sub>2</sub>. Reaction conditions: [NO]=[NH<sub>3</sub>]=400 ppm, [O<sub>2</sub>]=3%, balance N<sub>2</sub>, temperature: 323 K, total flow rate 2000 mL/min.

give a precise estimation of the depollution capacity of the catalysts.

Blank experiment used a gas stream containing 400 ppm NO, 400 ppm NH<sub>3</sub> and 3% O<sub>2</sub>. No variation of the NO concentration could be observed within 2 h of irradiation without the photocatalyst at 323 K. Moreover, no NO concentration change was found at either inlet or outlet when the Hg-arc lamp was turned off and the catalyst was present in the reactor. Therefore, it was concluded that the absence of the photocatalyst or the Hg-arc lamp did not cause the reduction of NO.

### 3. Results and discussion

#### 3.1. Photocatalytic activity

Fig. 2 shows the experiment results on the photocatalytic activity of various catalysts. At the beginning of the reaction, a very high NO conversion was observed for all prepared photocatalysts. The initial high conversion decreased quickly and approached to a steady state after half an hour operation. The high NO conversion at the beginning of the reaction is the result of the high initial rate of adsorption plus reaction of reactants [12].

The photocatalytic activity of Degussa P25 was a little higher than prepared TiO<sub>2</sub>. For samples with low silica loading, the photocatalytic activities were distinctly improved compared with pure TiO<sub>2</sub> and Degussa P25 at the steady state. When the Si doping concentration reached 3 at.%, the photocatalyst showed the highest NO conversion, which was 50% higher than that of pure TiO<sub>2</sub>. Then the photoactivity of catalyst was reduced with the increase of Si doping. The photocatalytic rate of catalyst is listed in Table 1. It decreases in the following sequence: Si(0.03)/TiO<sub>2</sub> > Si(0.01)/TiO<sub>2</sub> > Si(0.05)/TiO<sub>2</sub> > TiO<sub>2</sub>.

**Table 1**  
Photocatalytic rates and microstructure properties of TiO<sub>2</sub> and Si-doped TiO<sub>2</sub> samples

Sample	Photocatalytic rate (g/m <sup>2</sup> s)	Crystal diameter (nm) <sup>a</sup>	BET surface area (m <sup>2</sup> /g)	Pore volume (×10 <sup>-2</sup> cm <sup>3</sup> /g)
TiO <sub>2</sub>	0.18	9.7	148.5	7.16
Si(0.01)/TiO <sub>2</sub>	0.24	8.1	174.7	8.54
Si(0.03)/TiO <sub>2</sub>	0.27	8.2	191.7	9.43
Si(0.05)/TiO <sub>2</sub>	0.22	8.0	183.9	9.03

<sup>a</sup> Calculated by Scherrer's equation.

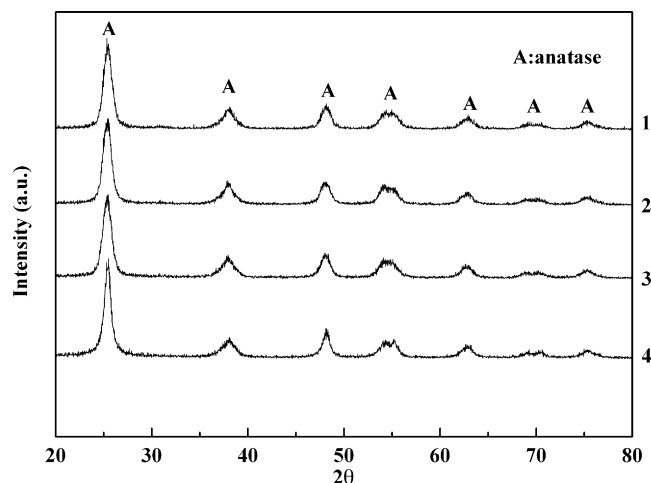


**Fig. 3.** The XRD patterns of pure and Si-doped TiO<sub>2</sub>: (1) TiO<sub>2</sub>; (2) Si(0.01)/TiO<sub>2</sub>; (3) Si(0.03)/TiO<sub>2</sub>; (4) Si(0.05)/TiO<sub>2</sub>.

The difference between undoped TiO<sub>2</sub> and Si-doped TiO<sub>2</sub> (Si(0.03)/TiO<sub>2</sub> was chosen as representative) on microstructure, surface state and optical properties would be discussed in detail in the following section.

#### 3.2. Microstructure properties

Fig. 3 shows the XRD patterns of TiO<sub>2</sub> and Si/TiO<sub>2</sub> photocatalysts. All samples shown in the figure had pure anatase phase and a good degree of crystallization. For samples containing silicon, no crystalline phase of silicon dioxide was observed. It indicates that silicon dioxide particles would be present in scarce amount or as very small crystals well dispersed over TiO<sub>2</sub> which was beyond XRD detection limitation [13].

On the basis of XRD diffractograms, the crystallite sizes of the catalysts were calculated using Scherrer's equation [14] ( $\Gamma = 0.94\lambda/L \cos \theta$ ;  $\Gamma$ : full width at the half maximum of the most intensive peak expressed in radians;  $L$ : diameter of the particle,  $\lambda = 1.54059 \text{ \AA}$ ;  $\theta$ : diffraction peak position) as listed in Table 1. All silica-doped TiO<sub>2</sub> catalysts had smaller sizes (in the range of 7.9–8.2 nm) than pure TiO<sub>2</sub>.

Table 1 also provides data about surface areas and pore volume of these catalysts. From the results it can be seen that the BET surface areas and the pore volume changed in the following order: TiO<sub>2</sub> < Si(0.01)/TiO<sub>2</sub> < Si(0.05)/TiO<sub>2</sub> < Si(0.03)/TiO<sub>2</sub>. All Si-doped TiO<sub>2</sub> samples have smaller crystal sizes, larger BET surface areas and larger pore volume than pure TiO<sub>2</sub>. These physico-chemical properties of the catalyst are believed to play an important role in the photoactivity improvement, since they provide higher active surface, higher illumination adsorption area and more effective contacts with the reactants.

TEM and HR-TEM were used to study the microstructure and crystallization of the hydrothermal-treated TiO<sub>2</sub> and Si/TiO<sub>2</sub> particles. As shown in Fig. 4, well-crystallized TiO<sub>2</sub> could be apparently

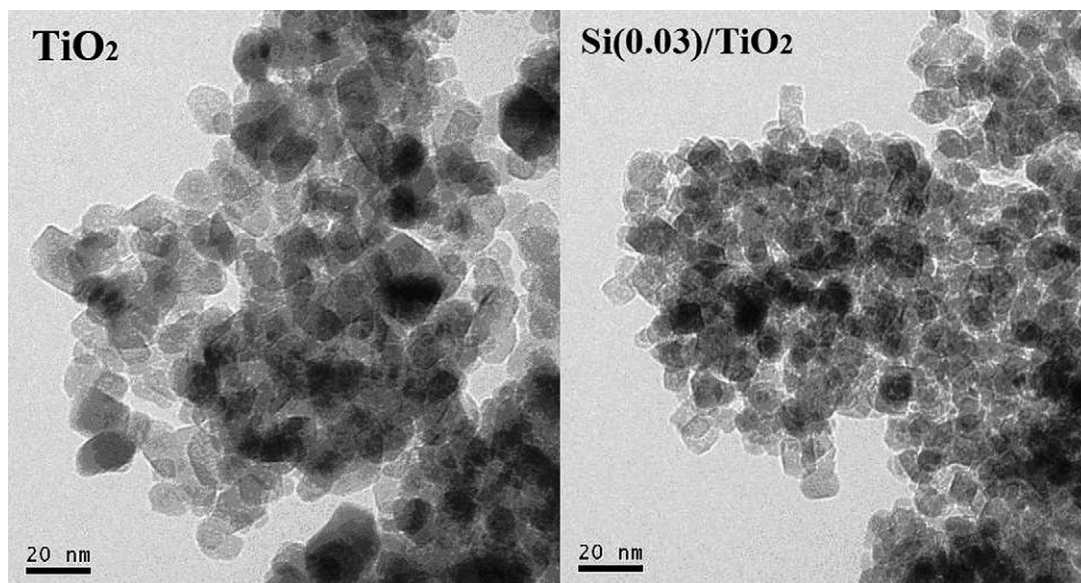


Fig. 4. TEM micrographs of  $\text{TiO}_2$  and  $\text{Si}(0.03)/\text{TiO}_2$  particles.

observed for both  $\text{TiO}_2$  and  $\text{Si}(0.03)/\text{TiO}_2$ . The primary particle size of  $\text{TiO}_2$  was about 10–20 nm while that of  $\text{Si}(0.03)/\text{TiO}_2$  was slightly smaller. Both of them were in agreement with the values of the crystallite size determined by XRD (9.7 and 8.2 nm, as shown in Table 1).

From the high-resolution TEM illustrated in Fig. 5, clear lattice fringes can be observed for both  $\text{TiO}_2$  and Si-doped  $\text{TiO}_2$  particles. The lattice plane distance was calculated to be 0.352 nm for  $\text{TiO}_2$  particles, which matched the (1 0 1) plane of  $\text{TiO}_2$  well (i.e. 0.3521 nm for the anatase [15]). The value of anatase interplanar distance determined for  $\text{Si}(0.03)/\text{TiO}_2$  particles was somewhat smaller (0.346 nm, shown by the right arrowhead in Fig. 5). Another lattice fringes with a lattice plane distance of about 0.239 nm is observed in Fig. 5 as shown by the left arrowhead, it was probably to be  $\text{SiO}_2$  particles (the interplanar distance of the (1 1 0) plane of  $\text{SiO}_2$  was reported to be 0.26 nm [16]).

Therefore, the results of TEM, XRD and BET indicate that Si doping in titania particle decreases the crystallite size by inhibiting the growth of  $\text{TiO}_2$  particles and helps to restrain the reduction of surface area at high calcination temperature.

### 3.3. XPS, FT-IR and $\text{NH}_3$ -TPD analysis

In order to identify the state of silicon species on the surface of  $\text{TiO}_2$ , the samples were examined by XPS spectroscopy. Si 2p spectra of  $\text{Si}(0.03)/\text{TiO}_2$  powder is shown in the inset of Fig. 6. The binding energy of Si 2p (101.6 eV) is smaller than that of  $\text{SiO}_2$  which was reported to be 103.4 eV [17]. This reduction should be due to an oxygen loss in  $\text{SiO}_2$ . Since Ti has greater affinity for oxygen than Si, some Si–O bands disappeared to promote the formation of Ti–O bands on the surface of Si-doped  $\text{TiO}_2$  [18]. That leads to an understoichiometry  $\text{SiO}_x$  ( $x < 2$ ) in Si-doped  $\text{TiO}_2$ , and consequently to a reduction in the binding energy of Si 2p. It can be the evidence of the formation of Si–O–Ti band in the Si-doped  $\text{TiO}_2$  sample.

From the Ti 2p spectrum of XPS shown in Fig. 7, we can see that the Ti 2p spectra consist only of  $\text{Ti}^{4+}$  peaks and no  $\text{Ti}^{3+}$  peaks both for  $\text{TiO}_2$  and Si-doped  $\text{TiO}_2$ . The binding energy of Ti 2p<sub>2/3</sub> peak for  $\text{Si}(0.03)/\text{TiO}_2$  is 458.65 eV, which is 0.2 eV greater than that of pure  $\text{TiO}_2$ . The decrease of the electron density around Ti atom is due to the greater electronegativity of Si via O acting on Ti [19]. The shield-

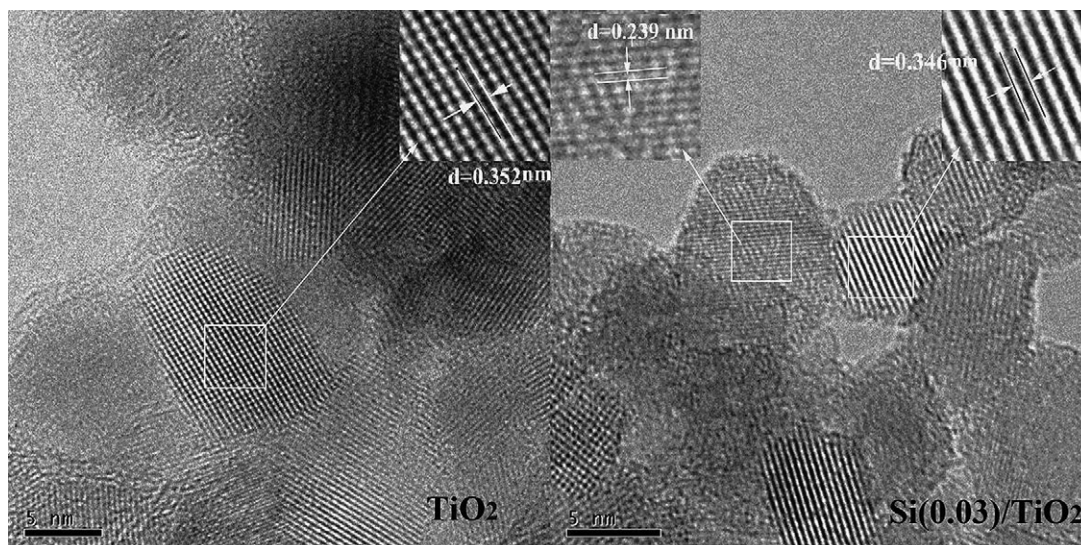


Fig. 5. HR-TEM micrographs of  $\text{TiO}_2$  and  $\text{Si}(0.03)/\text{TiO}_2$  particles.

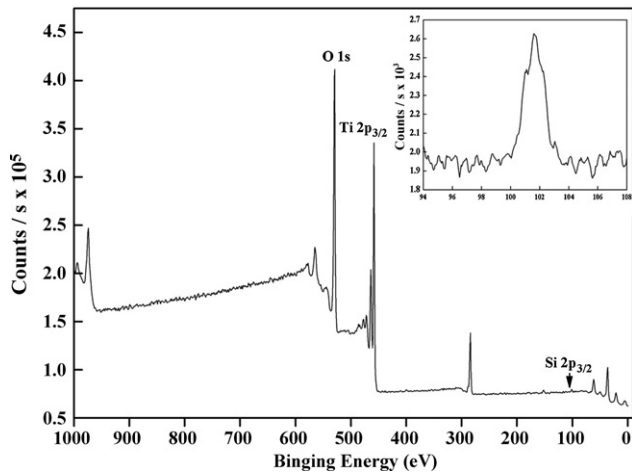


Fig. 6. XPS spectrum of Si-doped  $\text{TiO}_2$  (the  $\text{Si } 2p_{3/2}$  line is plotted in the inset).

ing effect is weakened, and then the binding energy is increased. This result further proves the formation of Ti–O–Si band on the surface of Si-doped  $\text{TiO}_2$ . Tanabe et al.'s [6] model had assumed that the dopant oxide's cation entered the lattice of host oxide and retained its original coordination number. A charge disbalance was created during this process and acidity sites were expected to be formed due to this disbalance. Therefore, the formation of Ti–O–Si band in Si/ $\text{TiO}_2$  was believed to develop more surface acidity. This surface acidity was thought to take the form of stronger surface hydroxyl groups which was validated by XPS result of O 1s peak as discussed in the following text (see Fig. 7 and Table 2).

The position and shape of O 1s peak of Si(0.03)/ $\text{TiO}_2$  is similar with that of pure  $\text{TiO}_2$  as illustrated in Fig. 7. The O 1s spectra give three distinct peaks. The two lower BE peaks are due to oxygen from  $\text{H}_2\text{O}$  and OH, whereas the highest BE peak is due to oxygen from  $\text{TiO}_2$ . Clearly, the surface hydroxyl concentration of Si(0.03)/ $\text{TiO}_2$  is much larger than that of pure  $\text{TiO}_2$  as listed in Table 2. Linsebigler et al. [20] had reported that hydroxyl groups on  $\text{TiO}_2$  surface would accept holes generated by illumination and produce hydroxyl radi-

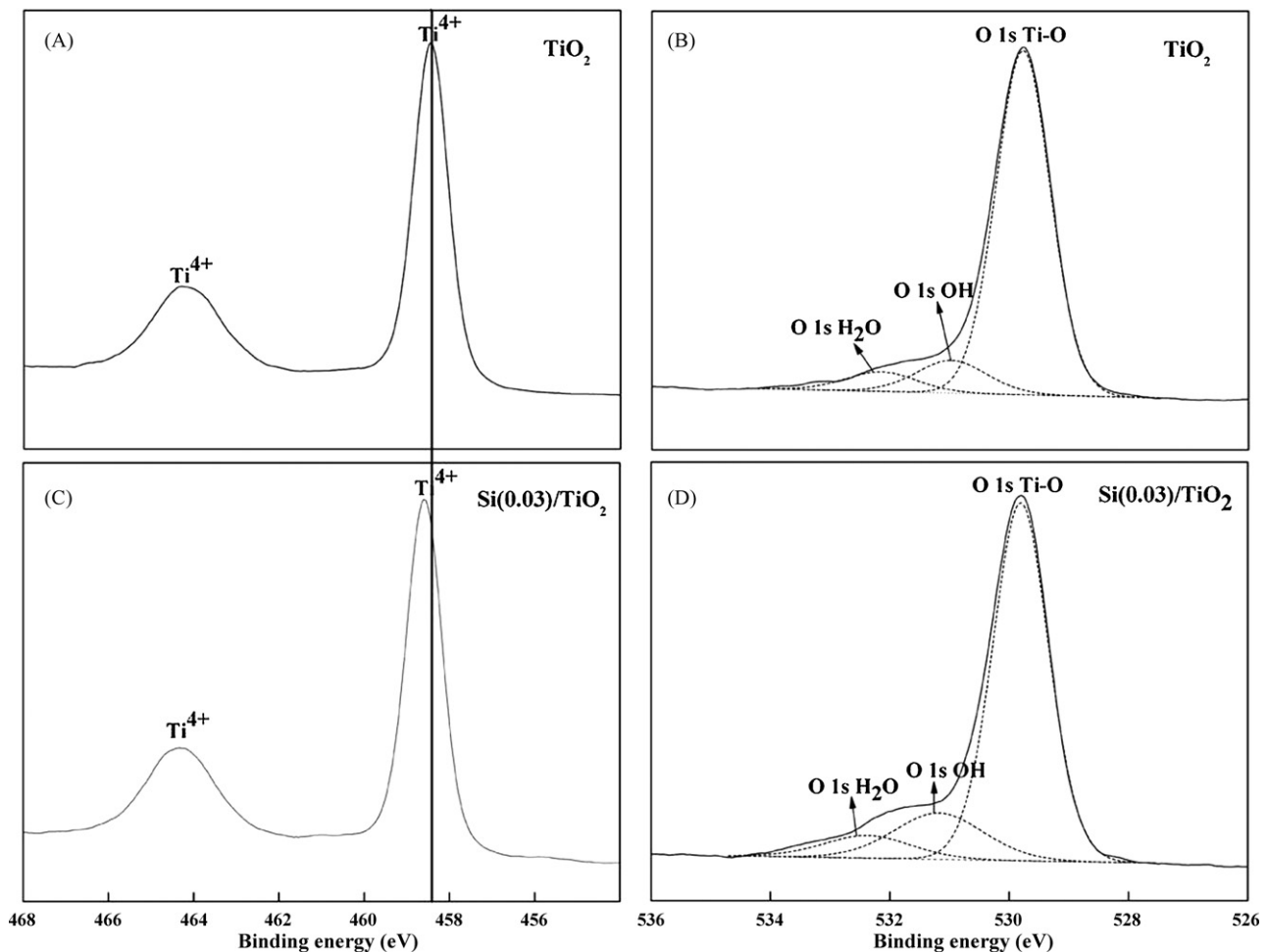


Fig. 7. Ti 2p and O 1s XPS spectra of  $\text{TiO}_2$  and Si(0.03)/ $\text{TiO}_2$  (A: Ti 2p for  $\text{TiO}_2$ ; B: O 1s for  $\text{TiO}_2$ ; C: Ti 2p for Si(0.03)/ $\text{TiO}_2$ ; D: O 1s for Si(0.03)/ $\text{TiO}_2$ ).

Table 2

The binding energies of O 1s in  $\text{TiO}_2$  and Si(0.03)/ $\text{TiO}_2$

	Samples					
	$\text{TiO}_2$			Si(0.03)/ $\text{TiO}_2$		
	Ti–O	OH	$\text{H}_2\text{O}$	Ti–O	OH	$\text{H}_2\text{O}$
Binding energy (eV)	529.78	530.98	532.16	529.81	531.18	532.37
Surface atomic concentrations (%)	44.63	5.53	3.32	40.52	8.47	4.05

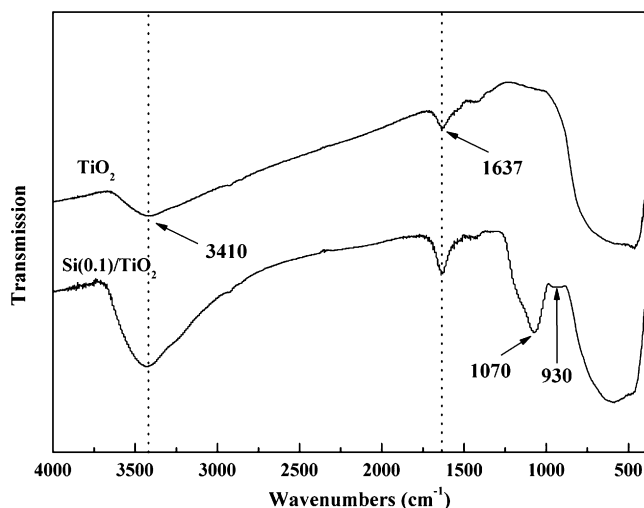


Fig. 8. FT-IR absorption spectra of  $\text{TiO}_2$  and Si-doped  $\text{TiO}_2$ .

cals which are strong oxidizing agents. Therefore, the redox reaction occurs more easily on the surface of  $\text{Si}(0.03)/\text{TiO}_2$ , which has a positive effect on NO catalytic reduction with  $\text{NH}_3$  [21].

Fig. 8 shows the FT-IR absorption spectrum of  $\text{TiO}_2$  and Si-doped  $\text{TiO}_2$ . The broad band around  $3410\text{ cm}^{-1}$  and the band at  $1637\text{ cm}^{-1}$  have been reported to correspond to the surface adsorbed water and hydroxyl groups [22]. The broad band around  $570\text{ cm}^{-1}$  is attributed to the Ti–O stretching vibrations of crystalline  $\text{TiO}_2$  phase. For  $\text{Si}(0.03)/\text{TiO}_2$ , there are two additional bands at about  $1070$  and  $930\text{ cm}^{-1}$  which were commonly accepted as the characteristic stretching vibration of Si–O–Si and Ti–O–Si bands in Ti- and Si-containing catalysts [19]. It further implies that not only Ti–O–Ti and Si–O–Si but also Ti–O–Si bands were formed during the hydrothermal process.

The amount and strength of the acid sites in the  $\text{TiO}_2$  and  $\text{Si}(0.03)/\text{TiO}_2$  were determined by  $\text{NH}_3$ -TPD. Fig. 9 shows the ammonia desorption patterns for  $\text{TiO}_2$  and  $\text{Si}(0.03)/\text{TiO}_2$ . Both of them show the presence of broadly distributed acid sites. The signal of  $\text{Si}(0.03)/\text{TiO}_2$  greatly increased compared to pure  $\text{TiO}_2$  which meant the density of acid sites was enhanced with Si doping. It was consistent with our forementioned conclusion that the formation of Ti–O–Si band would develop more acid sites.

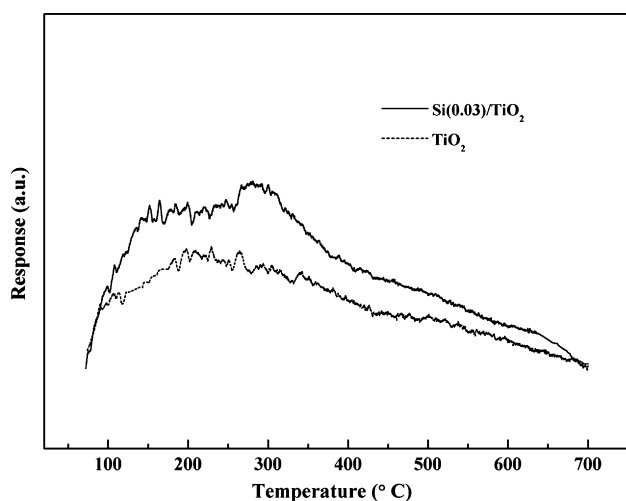


Fig. 9.  $\text{NH}_3$ -TPD spectra of  $\text{TiO}_2$  and  $\text{Si}(0.03)/\text{TiO}_2$ .

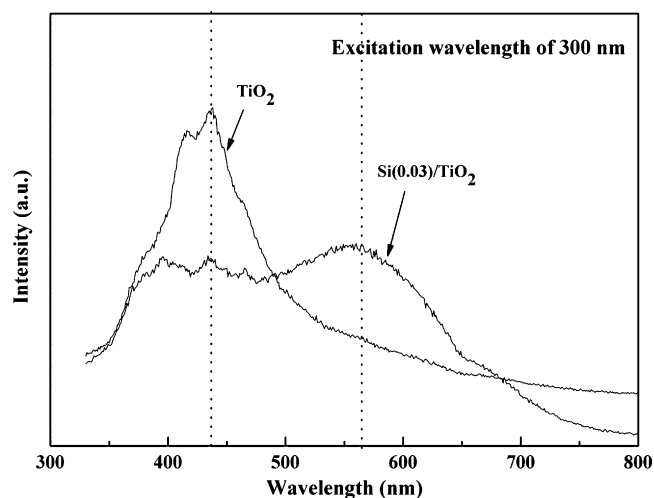


Fig. 10. PL spectra of  $\text{TiO}_2$  and Si-doped  $\text{TiO}_2$  particles.

### 3.4. Optical properties

Photoluminescence spectrum is an effective way to study the electronic structure, optical and photochemical properties of photocatalyst, by which information such as surface oxygen vacancies and defects, as well as the efficiency of charge carrier trapping, migration and transfer can be obtained. The room temperature PL spectra of  $\text{TiO}_2$  and  $\text{Si}(0.03)/\text{TiO}_2$  samples under the 300 nm UV ray excitation are shown in Fig. 10. Undoped  $\text{TiO}_2$  particles have two obvious PL peaks at about 420 and 438 nm, which mainly result from surface oxygen vacancies and defects of  $\text{TiO}_2$  particles [23].

$\text{Si}(0.03)/\text{TiO}_2$  particles exhibit totally different PL signal compared with undoped  $\text{TiO}_2$ . The excitonic PL intensity at about 438 nm decreased when an appropriate amount of Si was doped. It demonstrates that photo-induced electrons and holes can be efficiently separated for Si-doped  $\text{TiO}_2$ . It is because that hole traps such as the hydroxyl groups prevent electron–hole recombination and increase quantum yield [24]. Meanwhile, the excitonic PL signal at about 420 nm disappeared and a new broad PL band was formed at about 544 nm. It means that there is a new site for recombination of electrons and holes in  $\text{Si}(0.03)/\text{TiO}_2$  that is absent in  $\text{TiO}_2$ .

The UV–vis diffuse reflectance spectra of  $\text{TiO}_2$  and  $\text{Si}/\text{TiO}_2$  are shown in Fig. 11. From this figure, it can be seen that the UV light

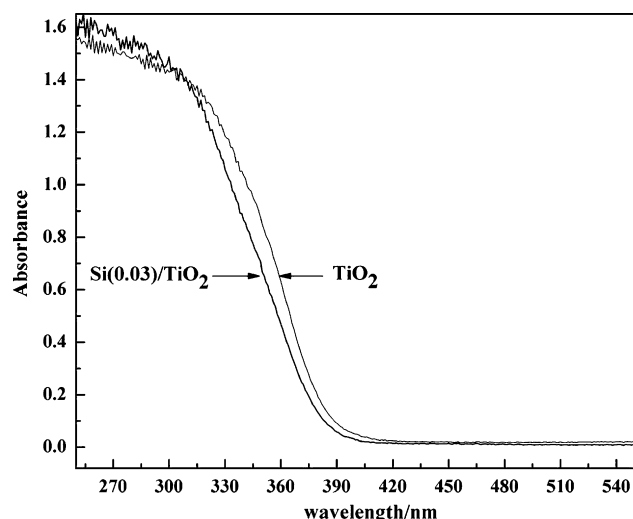


Fig. 11. UV–vis diffuse reflectance spectra of  $\text{TiO}_2$  and  $\text{Si}(0.03)/\text{TiO}_2$ .

below 380 nm could be absorbed and utilized in the photocatalytic reaction by TiO<sub>2</sub> and Si/TiO<sub>2</sub>. It also indicates that there is a blue shift in UV–vis spectrum of Si/TiO<sub>2</sub>. It is due to the quantization of band structure for titania, which is often observed when the particle size is less than several nanometers [25]. This quantized band structure confines the electrons photoexcited within the conduction band and retards the recombination rate [25]. Thus, the lifetime of electron and hole pairs were elongated and the corresponding photoactivity was improved.

All the results abovementioned indicate that Si doping greatly affected the catalyst's physicochemical characteristics and their photoactivity for NO reduction under UV irradiation. Si exists in the forms of Si–O–Si and Ti–O–Si which help to decrease the crystallite size by inhibiting the growth of TiO<sub>2</sub> particles and restrain the reduction of surface area at high calcination temperature. The formation of Ti–O–Si leads to the increase of acidity and increases surface hydroxyl groups concentration. These hydroxyl groups on TiO<sub>2</sub> surface can accept holes generated by illumination and produce hydroxyl radicals which were strong oxidizing agents. Therefore, redox reaction occurs more easily on the surface of Si-doped TiO<sub>2</sub> which has a positive effect on NO catalytic reduction with NH<sub>3</sub>. These hydroxyl groups prevent electron–hole recombination and increase quantum yield which is directly related to the photoactivity of catalysts.

#### 4. Conclusions

A series of Si-doped TiO<sub>2</sub> photocatalysts were prepared by hydrothermal process. The photocatalytic activity of Si-doped TiO<sub>2</sub> was higher than that of Degussa P25 and pure TiO<sub>2</sub> prepared by the same method when the molar ratio of Si to Ti was kept at 0.01–0.07. Among these catalysts, Si(0.03)/TiO<sub>2</sub> presented the highest NO conversion beyond 60% with NH<sub>3</sub> under UV irradiation at room temperature, which was 50% higher than undoped TiO<sub>2</sub>.

From the results of XRD, BET and TEM, it was clarified that all samples had pure anatase phase and that silicon dioxide particles were well dispersed on TiO<sub>2</sub>. Catalyst crystal size decreased from 9.7 to 7.9–8.2 nm and BET surface area increased from 150 to 175–192 m<sup>2</sup>/g with a low Si doping (1–10%). XPS and FT-IR results indicated that when small amount of silicon was doped into TiO<sub>2</sub>, Ti–O–Si band was formed and surface hydroxyl concentration was greatly increased. NH<sub>3</sub>-TPD showed that the total acidity of photocatalyst was increased with Si doping. A new photoelectron generating centre formation was proved by PL spectra for these Si-doped TiO<sub>2</sub>. The changes of physicochemical properties after the doping of Si contribute to the improvement of the photocatalytic reduction efficiency of NO.

#### Acknowledgements

The project is financially supported by the National Natural Science Foundation of China (NSFC-20577040) and New Century Excellent Scholar program of Ministry of Education of China (NCET-04-0549)

#### References

- [1] H. Bosch, F. Janssen, Formation and control of nitrogen oxides, *Catal. Today* 2 (1988) 369–379.
- [2] Z.B. Wu, B.Q. Jiang, Y. Liu, H.Q. Wang, R.B. Jin, DRIFT study of manganese/titania-based catalysts for low-temperature selective catalytic reduction of NO with NH<sub>3</sub>, *Environ. Sci. Technol.* 41 (2007) 5812–5817.
- [3] I.R. Subbotina, B.N. Shelimov, Selective photocatalytic reduction of nitric oxide by carbon monoxide over silica-supported molybdenum oxide catalysts, *J. Catal.* 184 (1999) 390–395.
- [4] K. Teramura, T. Tanaka, S. Yamazoe, K. Arakaki, T. Funabiki, Kinetic study of photo-SCR with NH<sub>3</sub> over TiO<sub>2</sub>, *Appl. Catal. B* 53 (2004) 29–36.
- [5] S. Yamazoe, T. Okumura, K. Teramura, T. Tanaka, Development of the efficient TiO<sub>2</sub> photocatalyst in photoassisted selective catalytic reduction of NO with NH<sub>3</sub>, *Catal. Today* 111 (2006) 266–270.
- [6] K. Tanabe, T. Sumiyoshi, K. Shibata, T. Kiyoura, J. Kitagawa, A new hypothesis regarding the surface acidity of binary metal oxides, *Bull. Chem. Soc. Jpn.* 47 (1974) 1064–1066.
- [7] B. Bonelli, M. Cozzolino, R. Tesser, M. Di Serio, M. Piumetti, E. Garrone, E. Santacesaria, Study of the surface acidity of TiO<sub>2</sub>/SiO<sub>2</sub> catalysts by means of FTIR measurements of CO and NH<sub>3</sub> adsorption, *J. Catal.* 246 (2007) 293–300.
- [8] R.W. Matthews, Kinetics and photocatalytic oxidation of organic solutes over titanium dioxide, *J. Catal.* 113 (1988) 549–555.
- [9] N. Enomoto, K. Kawasaky, M. Yoshida, X. Li, M. Uheara, J. Hojo, Synthesis of mesoporous silica modified with titania and application to gas adsorbent, *Solid State Ionics* 151 (2002) 171–175.
- [10] N. Hüsing, B. Launay, D. Doshi, G. Kickelbick, Mesostructured silica–titania mixed oxide thin films, *Chem. Mater.* 14 (2002) 2429–2432.
- [11] A.I. Kontos, I.M. Arabatzis, D.S. Tsoukderis, A.G. Kontos, M.C. Bernard, D.E. Petrakis, P. Falaras, Efficient photocatalysts by hydrothermal treatment of TiO<sub>2</sub>, *Catal. Today* 101 (2005) 275–281.
- [12] S. Devahasdin, C. Fan, J.K. Li, D.H. Chen, TiO<sub>2</sub> photocatalytic oxidation of nitric oxide: transient behavior and reaction kinetics, *J. Photochem. Photobiol. A* 156 (2003) 161–170.
- [13] Z.B. Wu, B.Q. Jiang, Y. Liu, W.R. Zhao, B.H. Guan, Experimental study on a low-temperature SCR catalyst based on MnOx/TiO<sub>2</sub> prepared by sol–gel method, *J. Hazard. Mater.* 145 (2007) 488–494.
- [14] Th.J. Singh, T. Mimani, K.C. Patil, S.V. Bhat, Enhanced lithium-ion transport in PEG-based composite polymer electrolyte with Mn<sub>0.03</sub>Zn<sub>0.97</sub>Al<sub>2</sub>O<sub>4</sub> nanoparticles, *Solid State Ionics* 154–155 (2002) 21–27.
- [15] S.Y. Chae, M.K. Park, S.K. Lee, T.Y. Kim, S.K. Kim, W.I. Lee, Preparation of size-controlled TiO<sub>2</sub> nanoparticles and derivation of optically transparent photocatalytic film, *Chem. Mater.* 15 (2003) 3326–3331.
- [16] J.X. Jiao, X. Qun, L.M. Li, Porous TiO<sub>2</sub>/SiO<sub>2</sub> composite prepared using PEG as template direction reagent with assistance of supercritical CO<sub>2</sub>, *J. Colloid Interf. Sci.* 316 (2007) 596–603.
- [17] C. Hu, Y.Z. Wang, H.X. Tang, Preparation and characterization of surface bond-conjugated TiO<sub>2</sub>/SiO<sub>2</sub> and photocatalysis for azo dyes, *Appl. Catal. B* 30 (2001) 277–285.
- [18] Y. Leprince-Wang, Study of the initial stages of TiO<sub>2</sub> growth on Si wafers by XPS, *Surf. Coat. Technol.* 150 (2002) 257–262.
- [19] X.L. Yan, H. Jing, D.G. Evans, X. Duan, Y.X. Zhu, Preparation, characterization and photocatalytic activity of Si-doped and rare earth-doped TiO<sub>2</sub> from mesoporous precursors, *Appl. Catal. B* 55 (2005) 243–252.
- [20] A.L. Linsebigler, G.Q. Lu, J.T. Yates Jr., Photocatalysis on TiO<sub>2</sub> surfaces: principles, mechanisms, and selected results, *Chem. Rev.* 95 (1995) 735–758.
- [21] K. Rahkamaa-Tolonen, T. Maunula, M. Lomma, M. Huuhtanen, R.L. Keiski, The effect of NO<sub>2</sub> on the activity of fresh and aged zeolite catalysts in the NH<sub>3</sub>-SCR reaction, *Catal. Today* 100 (2005) 217–222.
- [22] Z. Ding, G.Q. Lu, P.F. Greenfield, Role of the crystallite phase of TiO<sub>2</sub> in heterogeneous photocatalysis for phenol oxidation in water, *J. Phys. Chem. B* 104 (2000) 4815–4820.
- [23] L.Q. Jing, Y.C. Qu, B.Q. Wang, S.D. Li, B.J. Jiang, L.B. Yang, W. Fu, H.G. Fu, Review of photoluminescence performance of nano-sized semiconductor materials and its relationships with photocatalytic activity, *Sol. Energy Mater. Sol. Cells* 90 (2006) 1773–1787.
- [24] X.Z. Fu, L.A. Lark, Q. Yang, M.A. Anderson, Enhanced photocatalytic performance of titania-based binary metal oxides: TiO<sub>2</sub>/SiO<sub>2</sub> and TiO<sub>2</sub>/ZrO<sub>2</sub>, *Environ. Sci. Technol.* 30 (1996) 647–653.
- [25] K.Y. Jung, S.B. Park, Photoactivity of SiO<sub>2</sub>/TiO<sub>2</sub> and ZrO<sub>2</sub>/TiO<sub>2</sub> mixed oxides prepared by sol–gel method, *Mater. Lett.* 58 (2004) 2897–2900.